Implicit Active Contours Driven by Local Binary Fitting Energy

Chunming Li [1], Chiu-Yen Kao [2], John C. Gore [1], and Zhaohua Ding [1]

[1] Institute of Imaging Science
Vanderbilt University
Nashville, TN 37232-2310, USA

[2] Department of Mathematics
The Ohio State University
Columbus, OH 43210-1174, USA

Abstract

In this paper, we propose a novel region-based active contour model for image segmentation with a variational level set formulation. By introducing a local binary fitting energy, the proposed method is able to utilize accurate local image information for accurate recovery of desired object boundary. Our method is able to segment images with intensity inhomogeneity, weak object boundaries, and vessel-like structures. Comparison with typical region based active contour models, such as piecewise constant model and piecewise smooth model, shows the advantages of our method in terms of computational efficiency and accuracy. In addition, the proposed method has promising application for image denoising. Our method has been successfully applied to synthetic and real images in different modalities.

1. Introduction

Active contour models have been one of the most successful methods for image segmentation [1, 4, 6, 10, 19]. There are several desirable advantages of active contour models. First, active contour models can achieve sub-pixel accuracy of the object boundaries [18]. Second, various prior knowledge, such as shape and intensity distribution, can be easily incorporated into active contour models for robust image segmentation [3, 8, 16]. Third, the resultant contours/surfaces are quite regular, which are convenient for further applications, such as shape analysis, classification, and recognition.

The existing active contour models can be categorized into two classes: *edge-based models* [1, 6, 7, 9, 10] and *region-based models* [2, 12–15]. These two types of models both have their pros and cons, and the choice of them in applications depends on different characteristics of images.

Edge-based models utilize image gradient to stop the evolving contours on the object boundaries. Typical edge-based active contour models [1, 10] have an edge-based stopping term and a balloon force term to control the motion of the contour. The edge-based stopping term serves to stop the contour on the desired object boundary, but it only takes effect near the image edges, since it is computed from the image gradient. The balloon force term is introduced to push the active contour from its initial location that is far away from the desired object boundary, so that the initial contour can be placed in a larger range. However, appropriate choice of balloon force is sometimes difficult. If the balloon force is not large enough, the evolving contour may not able to pass some narrow part of the object, such as thin branches of vessels. If the balloon force is too large, the active contour is likely to pass through weak object boundary, where the image gradient is relatively small compared to the balloon force.

Region-based active contour models have the following advantages over edge-based models. First, region-based models do not utilize the image gradient and therefore has better performance for the image with weak object boundaries. Second, they are significantly less sensitive to the location of initial contours. One of the most popular region-based active contour models is Chan-Vese model [2]. This model has been successful for images with two regions, each having a distinct mean of pixel intensity. In [17], Vese and Chan extended their original model in [2] by using a multiphase level set formulation, in which multiple regions can be represented by multiple level set functions. These models are called *piecewise constant (PC) models*, since they assume that an image consists of *statistically homogeneous regions*, with intensities in each region being a constant up to certain noise. Based on this assumption, image segmentation is performed by minimizing an energy functional whose variables are the contours (or level set functions in level set formulations) and a given number of constants, which approximate the image intensities in each region. The PC models are successful for images with homogeneous regions. However, the regions of interest in images

are often not statistically homogeneous, and therefore the PC models are not applicable to those types of images.

To handle more general scenario, Vese and Chan [17] and Tsai *et al.* [15] proposed two similar region-based active contour models, aiming at minimization of Mumford-Shah functional [11]. In [17], Vese and Chan proposed a *piecewise smooth (PS)* model, which overcomes the limitation of their original work [2]. But these methods are computationally inefficient. The technique proposed by Tsai *et al.* [15] can address the segmentation of images with intensity inhomogeneity. However, the computation in their method is also expensive. As proposed in [15], one way to reduce the computational cost is to use a contour near the object boundaries as the initial contour. In their method, such initial contour is obtained by a preliminary segmentation using other active contour models, such as Chan and Vese's PC model. However, for images with intensity inhomogeneity, Chan-Vese model can result in a contour that is still far away from the object boundary. In this situation, their two-stage approach still cannot significantly reduce the computation cost.

In fact, intensity inhomogeneity occurs in many real images of different modalities. In particular, it is often seen in medical images, such as X-ray radiography/tomography and magnetic resonance (MR) images, due to technical limitations or artifacts introduced by the object being imaged. For example, intensity inhomogeneity typically appears in MR images (see Fig. 4(a) for example). The inhomogeneity in MR images arises from non-uniform magnetic field produced by radio-frequency coils as well as from object susceptibility. The degree of this inhomogeneity is worse for higher field imaging (e.g, 7T MR) which is being increasingly used in research. Therefore, overcoming the difficulty of segmentation due to image inhomogeneity is a main motivation of this paper.

In this paper, we propose a novel active contour model that is able to segment images with intensity inhomogeneity and multiple means of pixel intensity. Our method is based on a mild assumption that the image can be approximated locally by a binary image. By introducing a local binary fitting energy, the proposed method is able to incorporate local image intensity information into a region-based active contour model. This energy functional is further incorporated into a variational level set formulation without reinitialization. Therefore, our model has no need for reinitialization. Our method is able to segment images with non-homogeneous regions, weak object boundaries, and vessel-like structures.

The remainder of this paper is organized as follows. We first review some well known existing region-based models and their limitations in Section 1.1 and 1.2. The proposed method is introduced in Section 2. The implementation and results of our method are given in Section 3. This paper is summarized in Section 4.

1.1. Mumford-Shah functional for image segmentation

Let $\Omega \subset \Re^2$ be the image domain, and $u_0 : \Omega \to \Re$ be a given image function. In [11], Mumford and Shah formulated the image segmentation problem as follows: given an image I, find a contour C in Ω. They proposed the following energy functional:

$$F^{MS}(u, C) = \int_{\Omega} (u-I)^2 dxdy + \nu \int_{\Omega \setminus C} |\nabla u|^2 dxdy + \nu |C| \tag{1}$$

where $|C|$ is the length of contour C. The minimization of the above Mumford-Shah functionals results in an optimal contour C that segments the images, and a piecewise smooth image u approximating the original image u_0. In practice, it is difficult to minimize the functional (1), due to the unknown contour C of lower dimension and the non-convexity of the functional.

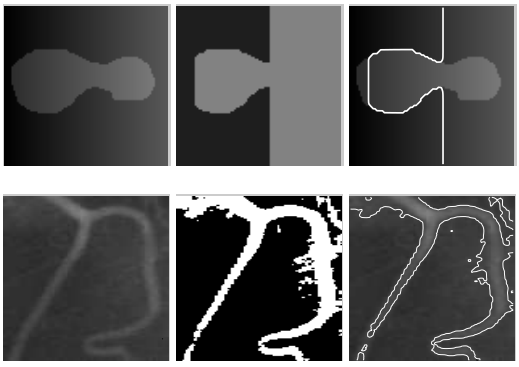

Figure 1. Error of thresholding and Chan-Vese model for images with intensity inhomogeneity. Column 1: Original images; Column 2: Thresholding results; Column 3: Results of Chan-Vese's PC model.

1.2. Region based active contour models

Chan and Vese [2] proposed an active contour model without using image gradient. For an image $I(x, y)$ on the image domain Ω, they propose to minimize the following energy

$$\begin{aligned} E^{CV}(C, c_1, c_2) &= \lambda_1 \int_{C_{in}} |I(\mathbf{x}) - c_1|^2 d\mathbf{x} \\ &+ \lambda_2 \int_{C_{out}} |I(\mathbf{x}) - c_2|^2 d\mathbf{x} \\ &+ \nu |C| \end{aligned} \tag{2}$$

where $in(C)$ and $out(C)$ represent the region inside and outside of the contour C, respectively, and c_1 and c_2 are two

constants that approximate the image intensity in $in(C)$ and $out(C)$. We call the first two terms in (2) the *global binary fitting energy*. This energy can be represented by a level set formulation, and then energy minimization problem can be converted to solving a level set evolution equation [2].

In the above Chan-Vese model, the constants c_1 and c_2 are introduced to fit the image intensities in the regions $in(C)$ and $out(C)$, respectively. Obviously, such global fitting will not be accurate if the image intensities in either $in(C)$ or $out(C)$ are not homogeneous. This is the reason why Chan-Vese model [2] cannot handle image inhomogeneity. Similarly, Vese and Chan's piecewise constant model in a multiphase level set framework [17] is still not suitable for images with intensity inhomogeneity.

1.3. Difficulty due to image inhomogeneity

The synthetic image and the real vessel image in Fig. 1 are typical examples of images with intensity inhomogeneity. For example, the intensity in the background decreases gradually from the top to the bottom in the vessel image. Moreover, part of the background (the upper left corner) has even higher intensities than part of the vessel (the lower left branch). The second column of Fig. 1 shows the results of thresholding for the two images. For the synthetic image in Fig. 1, a large part of the background is incorrectly identified as the foreground by segmentation using thresholding. For the vessel image, the thresholding also incorrectly label part of background pixels as the vessel, while a significant part of the vessel is missing. The third column of Fig. 1 shows the results of Chan-Vese model , which are similar to those of thresholding and therefore not correct.

1.4. Piecewise smooth models and their difficulties

The PS models proposed by Vese and Chan [15, 17] and Tsai *et al* [15] have overcome the difficulties of PC models in the presence of image inhomogeneity. Instead of approximating an image I by piecewise constant functions as in PC models, the PS model approximate the image by two smooth functions $u^-(\mathbf{x})$ and $u^+(\mathbf{x})$ in the subregions $\Omega^- = \{\mathbf{x} \in \Omega : \phi(\mathbf{x}) < 0\}$ (i.e., $in(C)$) and $\Omega^+ = \{\mathbf{x} \in \Omega : \phi(\mathbf{x}) > 0\}$ (i.e., $in(C)$), respectively. By definition, the functions u^- and u^+ are defined on two exclusive subregions Ω^- and Ω^+, respectively. However, the level set evolution equation derived to minimize the energy functional in the PS model is with respect to the level set function ϕ, which is defined on the full domain Ω. Therefore, there is an unavoidable step that extends u^- and u^+ to the full domain Ω. Moreover, the smoothness of the functions u^- and u^+ is due to the smoothing terms $\mu \int |\nabla u^-|^2 d\mathbf{x}$ and $\mu \int |\nabla u^+|^2 d\mathbf{x}$ in the energy functional in the PS model, from which two PDEs with respect to u^- and u^+ are derived and have to be solved for minimization of entire energy.

In summary, the minimization of the energy functional in PS model in level set formulation consists of the following three computational tasks. The first one is to solve the PDE of the main function ϕ by a sequence of iterations. Second, at every certain number of iterations for ϕ, the fitting functions u^- and u^+ have to be updated accordingly for the updated ϕ. Each update of u^- and u^+ is to solve two PDEs of them in the domain Ω^- and Ω^+, respectively. Third, the function u^- and u^+ have to be extended to the full domain Ω. In some situations, reinitialization is required to maintain stable evolution of ϕ. Obviously, the involved computation in PS model is expensive, which limit its applications in practice. We will introduce a new variational level set formulation, for which there is only one PDE to be solved. Moreover, there are no procedures of function extension and reinitialization in our method. The details are given in the rest of this paper.

2. Local binary fitting active contour model and its level set formulation

2.1. Active contours with local binary fitting energy

Consider a given vector valued image $\Omega \to \Re^d$, where $\Omega \subset \Re^n$ is the image domain, and $d \geq 1$ is the dimension of the vector $I(\mathbf{x})$. For gray level images, $d = 1$, for color images, $d = 3$. Let C be a contour in the image domain Ω. We define for each point $\mathbf{x} \in \Omega$ the following energy

$$\begin{aligned} E_{\mathbf{x}} &= \lambda_1 \int_{in(C)} K(\mathbf{x}-\mathbf{y})|I(\mathbf{y}) - f_1(\mathbf{x})|^2 d\mathbf{y} \\ &+ \lambda_2 \int_{out(C)} K(\mathbf{x}-\mathbf{y})|I(\mathbf{y}) - f_2(\mathbf{x})|^2 d\mathbf{y} \quad (3) \end{aligned}$$

where λ_1 and λ_2 are positive constants, and K is a weighting function with a localization property that $K(\mathbf{u})$ decreases and approaches zero as $|\mathbf{u}|$ increases, and $f_1(\mathbf{x})$ and $f_2(\mathbf{x})$ are two numbers that fit image intensities near the point $\mathbf{x}$. We call the point $\mathbf{x}$ the *center point* of the above integral, and the above energy the *local binary fitting (LBF) energy* around the center point $\mathbf{x}$. Since the above energy $E_{\mathbf{x}}$ depends on the center point $\mathbf{x}$, the contour C, and two fitting values $f_1(\mathbf{x})$ and $f_2(\mathbf{x})$, we denote (3) by $E^{LBF}_{\mathbf{x}}(C, f_1(\mathbf{x}), f_2(\mathbf{x}))$.

In this work, we choose the weighting function $K(\mathbf{x})$ as a Gaussian kernel

$$K_\sigma(\mathbf{x}) = \frac{1}{(2\pi)^{n/2}\sigma} e^{-|\mathbf{x}|^2/2\sigma^2}, \quad (4)$$

with a scale parameter $\sigma > 0$. It should be emphasized that the numbers f_1 and f_2 that minimize the energy (3) varies with the center point $\mathbf{x}$. The significance of such a spatially varying f_1 and f_2 makes our method essentially different from the Chan and Vese's piecewise constant model.

In the proposed model, the fitting energy in (3) is localized in the sense that the values f_1 and f_2 only fit the image intensities near each center point $\mathbf{x}$, due to the spatially varying weighting function K with the above localization property. This can be clearly explained as the following. Since the weighting function $K(\mathbf{x}-\mathbf{y})$ takes larger values at the points $\mathbf{y}$ near the center point $\mathbf{x}$, and it dramatically decreases to 0 as $\mathbf{y}$ goes away from $\mathbf{x}$, the image intensities at the points $\mathbf{y}$ near the point $\mathbf{x}$ have dominant influence on the values of f_1 and f_2 that minimize $E_{\mathbf{x}}^{LBF}(C, f_1, f_2)$ than the points $\mathbf{y}$ far away from the center point $\mathbf{x}$. And the image intensities at the points $\mathbf{y}$ far away from the center point $\mathbf{x}$ has almost no influence on the values of f_1 and f_2 that minimize the $E_{\mathbf{x}}^{LBF}(C, f_1, f_2)$, since the weighting function $K(\mathbf{x}-\mathbf{y})$ approaches zero for large distance $|\mathbf{x}-\mathbf{y}|$.

As mentioned above, the values f_1 and f_2 that minimize the LBF energy $E_{\mathbf{x}}^{LBF}(C, f_1, f_2)$ are functions of the center point $\mathbf{x}$ due to the spatially varying weighting function $K(\mathbf{x}-\mathbf{y})$. Obviously, for each center point $\mathbf{x}$, the local fitting energy $E_{\mathbf{x}}^{LBF}$ can be minimized when the contour C is exactly on the object boundary and the fitting values f_1 and f_2 are chosen optimally. This is based on a mild assumption that an image can be locally approximated by a binary image in a neighborhood of any point $\mathbf{x}$, which is satisfied by many typical real images. For instance, blood vessel images exhibit such a local binary pattern, as can be seen in Fig. 1.

However, the above energy $E_{\mathbf{x}}^{LBF}$ is defined locally for a center point $\mathbf{x} \in \Omega$. To find the entire object boundary, we must minimize $E_{\mathbf{x}}^{LBF}$ for all the center points $\mathbf{x}$ in the image domain Ω. This can be achieved by minimize the integral of $E_{\mathbf{x}}^{LBF}$ over all the center point $\mathbf{x}$ in the image domain Ω. So, we define the following energy functional

$$E(C, f_1, f_2) = \int_{\Omega} E_{\mathbf{x}}^{LBF}(C, f_1(\mathbf{x}), f_2(\mathbf{x}))d\mathbf{x} \quad (5)$$

This energy is computed from the image data I, so we call it an external energy. We will introduce some internal energy terms to regularize the contours.

2.2. Variational level set formulation of the model

In level set methods, a contour $C \subset \Omega$ is represented by the zero level set of a Lipschitz function $\phi : \Omega \to \Re$. With the level set representation, the energy functional $E^{LBF}(C, f_1(\mathbf{x}), f_2(\mathbf{x}))$ can be rewritten as

$$\begin{aligned} &E_{\mathbf{x}}^{LBF}(\phi, f_1, f_2) \\ &= \lambda_1 \int K_\sigma(\mathbf{x}-\mathbf{y})|I(\mathbf{y}) - f_1(\mathbf{x})|^2 H(\phi(\mathbf{y}))d\mathbf{y} \\ &+\lambda_2 \int K_\sigma(\mathbf{x}-\mathbf{y})|I(\mathbf{y}) - f_2(\mathbf{x})|^2 (1-H(\phi(\mathbf{y}))d\mathbf{y} \quad (6) \end{aligned}$$

where H is the Heaviside function. Thus, the fitting energy E in Eq. (5) can be written as

$$\begin{aligned} &E^{LBF}(\phi, f_1, f_2) = \int_{\Omega} E_{\mathbf{x}}^{LBF} d\mathbf{x} \\ &= \lambda_1 \int [\int K_\sigma(\mathbf{x}-\mathbf{y})|I(\mathbf{y}) - f_1(\mathbf{x})|^2 H(\phi(\mathbf{y}))d\mathbf{y}]d\mathbf{x} \\ &+\lambda_2 \int [\int K_\sigma(\mathbf{x}-\mathbf{y})|I(\mathbf{y}) - f_2(\mathbf{x})|^2 (1-H(\phi(\mathbf{y}))d\mathbf{y}]d\mathbf{x} \end{aligned} \quad (7)$$

In order to ensure stable evolution of the level set function ϕ, we add the distance regularizing term in Li *et al*'s variational level set formulation [9] to penalize the deviation of the level set function ϕ from a signed distance function. The deviation of the level set function ϕ from a signed distance function is characterized by the following integral

$$D(\phi) = \int_{\Omega} \frac{1}{2}(|\nabla\phi(\mathbf{x})| - 1)^2 d\mathbf{x} \quad (8)$$

To regularize the zero level contour of ϕ, we also need the length of the zero level curve (surface) of ϕ, which is given by

$$L(\phi) = \int_{\Omega} \delta(\phi(\mathbf{x}))|\nabla\phi(\mathbf{x})|d\mathbf{x} \quad (9)$$

Now, we define the entire energy functional

$$F(\phi, f_1, f_2) = E^{LBF}(\phi, f_1, f_2) + \beta D(\phi) + \nu L(\phi) \quad (10)$$

where β and ν are nonnegative constants.

In practice, the Heaviside function H in Eq. (6) is approximated by a smooth function H_ε defined by

$$H_\varepsilon(x) = \frac{1}{2}[1 + \frac{2}{\pi}\arctan(\frac{x}{\varepsilon})] \quad (11)$$

The derivative of H_ε is the following smooth function

$$\delta_\varepsilon(x) = H'_\varepsilon(x) = \frac{1}{\pi}\frac{\varepsilon}{\varepsilon^2 + x^2} \quad (12)$$

By replacing H and δ in (7) and (9) with H_ε and δ_ε, the energy functionals E^{LBF} and L are regularized as E_ε^{LBF} and L_ε. As in [2, 17], we choose $\varepsilon = 1.0$ for good approximation of H and δ by H_ε and δ_ε. Thus, the energy functional $F(\phi, f_1, f_2)$ in (10) is approximated by

$$F_\varepsilon(\phi, f_1, f_2) = E_\varepsilon^{LBF}(\phi, f_1, f_2) + \beta D(\phi) + \nu L_\varepsilon(\phi) \quad (13)$$

This is the energy functional we will minimize to find the object boundary.

2.3. Gradient Descent Flow

For a fixed level set function ϕ, we minimize the functional $F_\varepsilon(\phi, f_1, f_2)$ in (13) with respect to the functions $f_1(\mathbf{x})$ and $f_2(\mathbf{x})$. By calculus of variations, it can be shown that the functions $f_1(\mathbf{x})$ and $f_2(\mathbf{x})$ that minimize

$F_\varepsilon(\phi, f_1, f_2)$ for a fixed function ϕ satisfy the following Euler-Lagrange equations:

$$\int K_\sigma(\mathbf{x}-\mathbf{y})H_\varepsilon(\phi(\mathbf{y}))(I(\mathbf{y})-f_1(\mathbf{x}))d\mathbf{y}=0 \quad (14)$$

and

$$\int K_\sigma(\mathbf{x}-\mathbf{y})[1-H_\varepsilon(\phi(\mathbf{y}))](I(\mathbf{y})-f_2(\mathbf{x}))d\mathbf{y}=0 \quad (15)$$

From (14) and (15), it follows

$$f_1(\mathbf{x})=\frac{K_\sigma(\mathbf{x})*[H_\varepsilon(\phi(\mathbf{x}))I(\mathbf{x})]}{K_\sigma(\mathbf{x})*H_\varepsilon(\phi(\mathbf{x}))} \quad (16)$$

and

$$f_2(\mathbf{x})=\frac{K_\sigma(\mathbf{x})*[(1-H_\varepsilon(\phi(\mathbf{x})))I(\mathbf{x})]}{K_\sigma(\mathbf{x})*[1-H_\varepsilon(\phi(\mathbf{x}))]} \quad (17)$$

which minimize the energy functional $F_\varepsilon(\phi, f_1, f_2)$ for a fixed ϕ. Note that the denominators in (16) and (17) are always positive, due to the fact that $H_\varepsilon(\phi) > 0$ and $1 - H_\varepsilon(\phi) > 0$ by the definition of H_ε in (11).

Keeping f_1 and f_2 fixed, and minimizing the energy functional $F_\varepsilon(\phi, f_1, f_2)$ with respect to ϕ, we derive the gradient descent flow:

$$\begin{aligned}\frac{\partial\phi}{\partial t} &= -\delta_\varepsilon(\phi)(\lambda_1 e_1-\lambda_2 e_2)+\nu\delta_\varepsilon(\phi)\mathrm{div}\left(\frac{\nabla\phi}{|\nabla\phi|}\right)\\ &+ \beta\left(\nabla^2\phi-\mathrm{div}\left(\frac{\nabla\phi}{|\nabla\phi|}\right)\right) \quad (18)\end{aligned}$$

where δ_ε is the smooth Dirac function given by (12), and e_1 and e_2 are the functions as below

$$e_1(\mathbf{x})=\int_\Omega K_\sigma(\mathbf{y}-\mathbf{x})|I(\mathbf{x})-f_1(\mathbf{y})|^2 d\mathbf{y} \quad (19)$$

and

$$e_2(\mathbf{x})=\int_\Omega K_\sigma(\mathbf{y}-\mathbf{x})|I(\mathbf{x})-f_2(\mathbf{y})|^2 d\mathbf{y} \quad (20)$$

where f_1 and f_2 are given by (16) and (17), respectively. The above equation (18) is the proposed implicit active contour model in this paper.

2.4. Advantages of our model

In contrast to PS model [17], in our model, it is not necessary to regularize the fitting function f_1 and f_2. It fact, it is easy to prove that the functions f_1 and f_2 minimizing the functional (13) is given by (16) and (17), which are smooth functions due to the Gaussian convolutions in the derived formula (16) and (17). Moreover, there is no need of extension of f_1 and f_2 in our model, they are naturally defined on the full domain Ω.

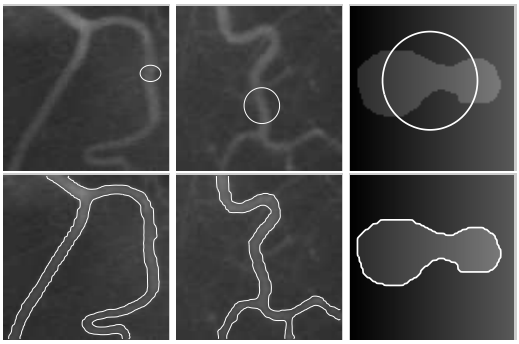

Figure 2. Application to two real blood vessel images and a synthetic image. Upper row: Original images and initial contours. Lower row: Final contours.

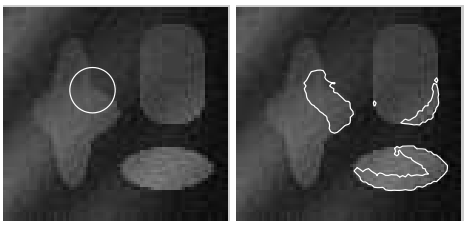

(a) Initial contour. (b) 5 iterations.

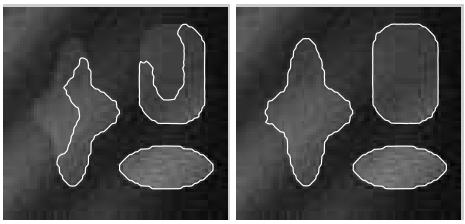

(c) 15 iterations. (d) 60 iterations.

Figure 3. Application to a noisy synthetic image.

Another advantage of our model is that no reinitialization is necessary in our method, due to the distance regularizing term (8). Moreover, our method with this distance regularizing term allows for flexible initialization of level set function ϕ. For example, we can simply initialize ϕ as a binary function, which takes a constant value c_0 in a region R_0 and $-c_0$ outside of R_0, where R_0 can be an arbitrarily given subset in the image domain Ω. Such simple initialization is not only efficient, but also has other desirable advantages, which we will demonstrate in Section 3.

3. Implementation and results

To compute the function f_1 and f_2 given by Eq. (16) and (17), we use the efficient FFT to compute the four convolution operations. The term $\lambda_1 e_1 - \lambda_2 e_2$ in (18) can be written as a linear combination of three convolutions, and is also computed by FFT in our current implementation. Note

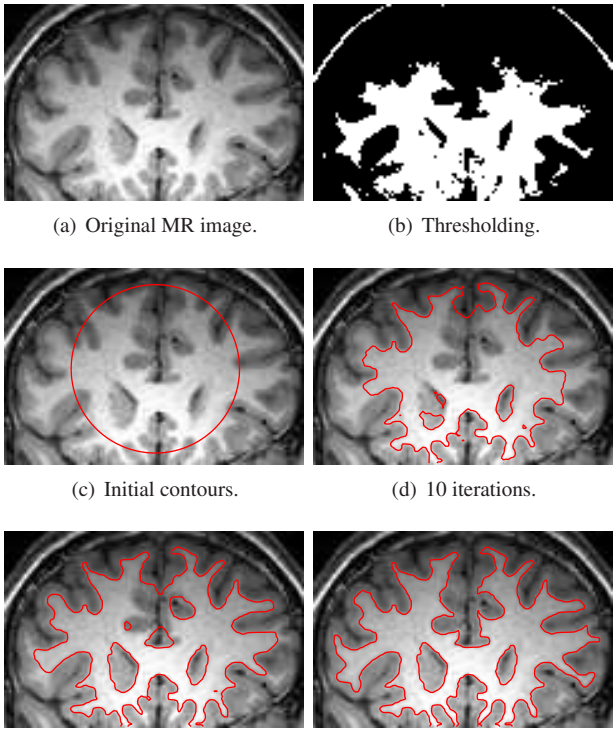

(a) Original MR image. (b) Thresholding.

(c) Initial contours. (d) 10 iterations.

(e) 50 iterations. (f) 200 iterations.

Figure 4. Application to white matter segmentation for MR image.

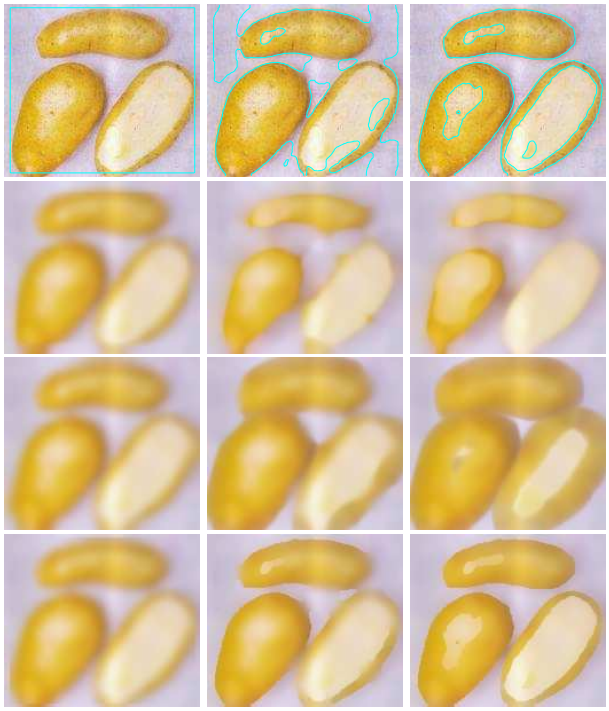

Figure 5. Results for a real color image of potatoes. Row 1: Contours on the original image; Row 2: Image f_1; Row 3: Image f_2; Row 4: Fitting image $H_\varepsilon(\phi)f_1 + (1 - H_\varepsilon(\phi))f_2$.

that there are more efficient algorithm than FFT for performing convolution [5]. All the partial derivatives $\frac{\partial \phi}{\partial x}$ and $\frac{\partial \phi}{\partial y}$ in (18) are approximated using standard finite difference scheme in [2].

3.1. Results for synthetic and real images

Our method has been applied to synthetic and real images of different modalities. Some examples are shown in Fig. 2, 3 4, and 5. We use the same parameters of $\nu = 0.001 \times 255^2$, time step $\tau = 0.1$, $\beta = 1.0$, and $\sigma = 3.0$, $\lambda_1 = \lambda_2 = 1.0$ for all the images in this paper, except the one in Fig. 4, for which we set $\nu = 0.003 \times 255^2$, $\lambda_1 = 1.0$ and $\lambda_2 = 2.0$. The level set is initialized as the binary function introduced in Section 2.4.

This work was originally motivated by our research on medical image segmentation. We first show the results of our method for the two blood vessel images in the third and fourth rows in Fig. 2. In these images, both the background and the vessels exhibit obvious intensity inhomogeneity, and part of the vessel boundaries in these two images are quite weak. The image in the third column is the same synthetic image in Fig. 1, for which the PC model fails to segment the object correctly. Fig. 2 show desirable results of our method for these challenging images. Fig. 3 shows a synthetic image contaminated with high level noise. It is clearly seen that the intensities are not homogeneous in either the background or the three objects. Our method successfully extracts the object boundaries in this image.

Fig. 4(a) shows the result for a coronal slice of an MR image of human brain. The region of our interest is the white matter in this image. However, this image shows obvious intensity inhomogeneity in the white matter, as can be seen clearly in Fig. 4(a). In fact, the intensity of white matter in the upper part is even smaller than that of the gray matter in the lower part. We first show a thresholding result in Fig. 4(b), which is obviously not correct. As we will show later, the PS model also have difficulty for this type of images. The second and the third rows show the evolution of the active contour in our model. Obviously, our method is able to segment the white matter in this image successfully, as shown in the lower right figure in Fig. 4.

The proposed method has also been applied to 3D magnetic resonance angiography (MRA) images for segmentation of cerebral vasculature. For example, Fig. 6(a) shows the MIP of a 3D MRA image. The image size is $300 \times 300 \times 60$ voxels with spacing of $0.195mm \times 0.195mm \times 0.5mm$. For this 3D image, we use the parameters $\lambda = 0.01 \times 255^2$, $\tau = 0.1$, $\beta = 1.0$, and $\sigma = 2.0$. The final surface obtained by our method is shown in Fig. 6(b).

Since our method is formulated for vector valued images,

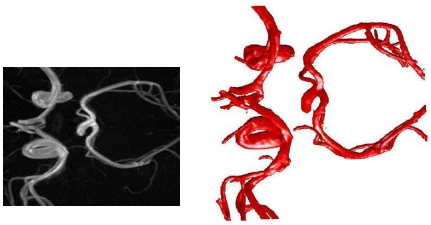

(a) MIP (b) Final surface of our method

Figure 6. Application to 3D MRA image segmentation.

it can be readily applied to color images. Fig 5 shows the results for a real color image of potatoes, which demonstrates the joint segmentation and denoising by using the LBF model. The first row plots the active contours on the original images from its initial to converged state. The second and third rows show the corresponding fitting image f_1 and f_2, computed by (16) and (17) respectively.

3.2. Image denoising by local binary fitting

As a natural application of our LBF model, the final fitting functions f_1 and f_2 and the level set function ϕ can be used for image denoising. We define the following fitting image

$$f = H_\varepsilon(\phi) f_1 + (1 - H_\varepsilon(\phi)) f_2 \tag{21}$$

The above computed image f can be used to approximate the original image while reducing the noise.

The fourth row in Fig. 5 shows the evolution of the fitting image f computed by (21). When the level set function ϕ converges, the fitting image f (shown in the right most images in the fourth row) fits the original image very well with noise significantly reduced. Moreover, the features in the original image, such as the boundaries of meaningful regions are enhanced.

3.3. A few remarks

As mentioned in Section 2.4, our model allows flexible initialization of level set function. With the binary initialization introduced in Section 2.4, the level set function ϕ can more easily develop new contours (zero level contours), which is necessary for segmentation of multiple separate objects (see Fig. 3 for example) or objects with holes.

In situations where only one region is of interest, such as the white matter in Fig. 4, we can choose larger weight ν of the length term to prevent the emergence of new contour. For the MR image, we use $\nu = 0.003 * 255^2$. Note that, the image in the second vessel image in Fig. 2 includes some minor vessels/branchs that are not detected by using the above given set of parameters. To detect those minor structures, we can choose a smaller value of ν.

Note that, the distance regularizing term in our model is necessary for stable curve evolution and accurate computation. In general, we suggest to use the distance regularizing term with coefficient $\beta = 1.0$.

3.4. Comparison with piecewise smooth model

The results of Chan and Vese's piecewise constant model (shown in Fig. 1) and the results of our method (Fig. 2) have demonstrated the advantage of our method. Since the PS models outperform other standard active contour models in the presence of image inhomogeneity, we focus on comparing our model with PS model in terms of the computational efficiency and accuracy.

We have implemented Vese and Chan's PS model in [17]. In our implementation of the PS model in [17], reinitialization is required. Without reinitialization, the active contours move very slowly, or even stop moving after a few iterations. By contrast, due to the distance regularizing term (8) proposed by Li *et al* [9] in our LBF energy functional (13), no reinitialization is necessary.

Fig. 7 shows the results of our and Vese-Chan's methods using the same initial contours. The upper and the lower rows show the results of our method and Vese-Chan method, respectively. The CPU time for these images are listed in Table 1. The CPU time is recorded for our Matlab code that was run on a Dell Dimension 4600 PC, with Pentium 4 processor, 2.80 GHz, 1GB RAM, with Matlab 6.5 on Windows XP. From Table 1, it is obvious that our model is significantly faster than the PS model. For the images in Fig. 7), our model is about 15 to 40 times faster than the PS model.

In terms of accuracy, the results for the first four images show that our model and PS model have similar final results. Note that the result of PS model in the second column was obtained by carefully choosing an initial contour (the two object boundaries on the right were missing when using the initial contour in Fig. 3(a) for the PS model). For the MR image, our method extracts the white matter boundary accurately without generating unwanted contours that are seen in the result of PS model. We can see that the final contour of the PS model is partly attracted to the boundary of gray matter, and therefore lose some part of white matter boundary. Certainly, by tuning the parameter ν, the PS model can also avoid those unwanted contours, but it comes at the cost of further losing fine details in the white matter boundary. The right most column in Fig. 7 is an enlarged view of the lower left portion of the figures in the fifth column, which shows relatively more accurate recovery of the desired object boundaries by our method, compared with the PS model. The accuracy of our method is due to its ability of utilizing local image information by the local binary fitting framework.

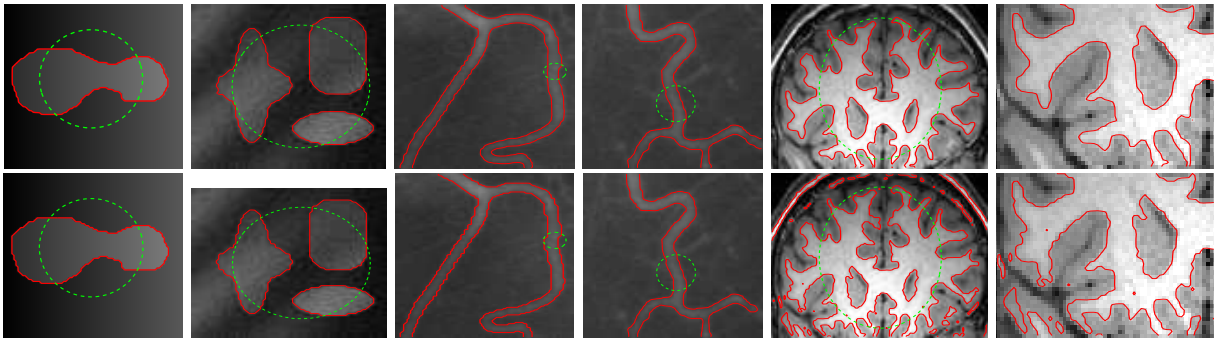

Figure 7. Comparison of our method with PS model. The initial contours and the final contours are plotted as the dashed green contours and solid red contours, respectively. Upper row: The results of our method; Lower row: The results of PS model.

	Img1	Img2	Img3	Img4	Img5
LBF	1.78	2.42	25.52	11.85	9.81
PS	39.92	101.89	398.45	203.03	120.52

Table 1. CPU time (in second) for LBF model and Vese-Chan's PS model for the images in Fig. 7 in the same order.

4. Conclusions and future work

In this paper, we propose a novel region-based active contour model for image segmentation with a variational level set formulation. By introducing a local binary fitting energy, the proposed method is able to utilize accurate local image information for accurate recovery of desired object boundary. Our method is able to segment images with non-homogeneous regions, weak object boundaries, and vessel-like structures. Comparison with typical region based active contour models shows the advantages of our method in terms of accuracy and efficiency. In addition, the proposed method has promising application for image denoising. In our future work, we will extend our method to handle regions with triple junctions. This could be achieved by using a multiphase level set framework. In addition, our current algorithm will be implemented with narrow band techniques to further speed up the computation.

References

[1] V. Caselles, R. Kimmel, and G. Sapiro. Geodesic active contours. *Int'l J. Comp. Vis.*, 22:61–79, 1997.

[2] T. Chan and L. Vese. Active contours without edges. *IEEE Trans. Imag. Proc.*, 10:266–277, 2001.

[3] T. Chan and W. Zhu. Level set based shape prior segmentation. In *IEEE Conference on Computer Vision and Pattern Recognotion (CVPR).*, volume II, pages 1164–1170, 2005.

[4] L. Cohen and I. Cohen. Finite-element methods for active contour models and balloons for 2-D and 3-D images. *IEEE Trans. Patt. Anal. Mach. Intell.*, 15:1131–1147, 1993.

[5] R. Deriche. Using canny's criteria to derive a recusively implemented optimal edge detector. *Int'l J. Comp. Vis.*, 1:167–187, 1987.

[6] M. Kass, A. Witkin, and D. Terzopoulos. Snakes: active contour models. *Int'l J. Comp. Vis.*, 1:321–331, 1987.

[7] R. Kimmel, A. Amir, and A. Bruckstein. Finding shortest paths on surfaces using level set propagation. *IEEE Trans. Patt. Anal. Mach. Intell.*, 17:635–640, 1995.

[8] M. Leventon, W. Grimson, and O. Faugeras. Statistical shape influence in geodesic active contours. In *IEEE Conference on Computer Vision and Pattern Recognotion (CVPR).*, volume I, pages 316–323, 2000.

[9] C. Li, C. Xu, C. Gui, and M. D. Fox. Level set evolution without re-initialization: A new variational formulation. In *IEEE Conference on Computer Vision and Pattern Recognotion (CVPR).*, volume 1, pages 430–436, 2005.

[10] R. Malladi, J. A. Sethian, and B. C. Vemuri. Shape modeling with front propagation: a level set approach. *IEEE Trans. Patt. Anal. Mach. Intell.*, 17:158–175, 1995.

[11] D. Mumford and J. Shah. Optimal approximations by piecewise smooth functions and associated variational problems. *Commun. Pure Appl. Math.*, 42:577–685, 1989.

[12] N. Paragios and R. Deriche. Geodesic active regions and level set methods for supervised texture segmentation. *Int'l J. Comp. Vis.*, 46:223–247, 2002.

[13] R. Ronfard. Region-based strategies for active contour models. *Int'l J. Comp. Vis.*, 13:229–251, 1994.

[14] C. Samson, L. Blanc Feraud, G. Aubert, and J. Zerubia. A variational model for image classification and restoration. *IEEE Trans. Patt. Anal. Mach. Intell.*, 22(5):460–472, 2000.

[15] A. Tsai, A. Yezzi, and A. S. Willsky. Curve evolution implementation of the mumford-shah functional for image segmentation, denoising, interpolation, and magnification. *IEEE Trans. Imag. Proc.*, 10:1169–1186, 2001.

[16] A. Tsai, A. J. Yezzi, W. M. W. III, C. Tempany, D. Tucker, A. Fan, W. E. L. Grimson, and A. S. Willsky. A shape-based approach to the segmentation of medical imagery using level sets. *IEEE Trans. Med. Imaging*, 22:137–154, 2003.

[17] L. Vese and T. Chan. A multiphase level set framework for image segmentation using the mumford and shah model. *Int'l J. Comp. Vis.*, 50:271–293, 2002.

[18] C. Xu, D. Pham, and J. Prince. Image segmentation using deformable models. In Unknown, editor, *Handbook of Med. Imaging, Med. Imag. Proc. and Anal.*, volume 2, pages 129–174. SPIE Press, 2000.

[19] C. Xu and J. Prince. Snakes, shapes, and gradient vector flow. *IEEE Trans. Imag. Proc.*, 7:359–369, 1998.